A&A 451, 1081–1089 (2006)
DOI: 10.1051/0004-6361:20047133

Astronomy & Astrophysics

Dynamics of the solar granulation

IX. A global approach

A. Nesis, R. Hammer, M. Roth, and H. Schleicher

Kiepenheuer-Institut für Sonnenphysik, Schöneckstr. 6, 79104 Freiburg, Germany
e-mail: nesis@kis.uni-freiburg.de

Received 23 January 2004 / Accepted 5 December 2005

ABSTRACT

Based on a series of spectrograms taken with the German Vacuum Tower Telescope (VTT) at the Observatorio del Teide (Tenerife), we study the temporal evolution of granular dynamics and energy transport in the photospheric layers. We consider the ensemble of the granules cut by the spectrograph slit, modulated by wave motion, as a complex system. We describe this ensemble by the rms of the fluctuations of the observables along the slit: continuum intensity I, gas velocity v measured from line center Doppler shifts with respect to the mean profile, and line width w. The history of the rms of the observables v and w reflects the dynamical change of the system over the 20 min observation time. We find a burst-like change for both observables. However, the cross-correlation between I and v remains virtually constant, with the exception of two gaps. Using six lines of different strength we measure the rms of v in the deep photospheric layers. On the basis of this v variation we derive an upper limit of the kinetic energy flux as a function of height in the photosphere for different times during the observation. The shape of the variation with height is constant over time. A limit for the convective enthalpy flux is calculated using the temperature variations of our earlier models. Its shape remains the same over time. Taken together, these results quantify the different roles that the lower and higher photospheric layers play in the energetics of convective overshoot.

Key words. Sun: photosphere – Sun: granulation

1. Introduction

The dynamics of solar granulation is crucial for the physical state of the photospheric layers. The intensity and velocity of granular structures not only reflect the physics of the upper convective layers but also have an effect on the higher layers, transferring energy and momentum (for a recent review see Muller 1999).

We therefore use high quality spectrograms to study the spreading of granular structures into the higher photospheric layers. Nesis et al. (1988) addressed this question and showed with a coherence analysis the breakdown of similarity between the small-scale intensities of the continuum level and of the layers above. They interpreted this as observational evidence for the relevance of the dynamics of the deep overshoot layers for small continuum intensity structures.

An important aspect of granular overshooting is the change of the convective velocity with height within the stable layers lying above. Its shape reflects the distribution of the granular velocity within the deep photospheric regime and gives insight into the extension of the upper convective super-adiabatic layers.

By observations and by applying the "weighting function" formalism iteratively, Nesis & Mattig (1989) calculated a parametric model of velocity as a function of height for the deep photospheric layers. The shape of the model velocity function shows a steep drop with height down to a minimum at ≈170 km above $\tau_{500} = 1$ and a moderate rise in the higher layers.

Komm et al. (1991a,b) addressed the evolution of the various granular intensity and velocity scales in the photosphere. They found that the deep photosphere is in fact divided into two regions dominated by different scales. They showed that the scales and motions associated with granular velocities decay within the first 170 km above the $\tau_{500} = 1$ layer. This behavior was confirmed by Borrero & Bellot Rubio (2002) in a two-component model with distinct velocities of granules and intergranules.

Observations taken at the VTT, Observatorio del Teide (Tenerife), also revealed a clear difference in the penetration of small and large granular scales into the overlying photospheric layers (cf. Nesis et al. 1997).

The organization as well as the evolution of the spatial granular patterns are signs of underlying dynamics, which manifest themselves in the time evolution of the granulation as well. Both spatial structure and temporal evolution must be intrinsic properties of the granulation dynamics.

In a recent paper Nesis et al. (2002) provided observational evidence for time scales that characterize the temporal behavior of the gas properties velocity v measured from Doppler shifts, line width w and continuum intensity I. The traces of the granular observables with time in the corresponding time-maps revealed the dynamical evolution of *individual* granules intersected by the spectrograph slit.

At the solar surface, dynamical events like merging or splitting of turbulent regions as well as strong upward or downward velocities provide evidence for violent processes in the underlying super-adiabatic layers (cf. Nesis et al. 2003; Skartlien 1998). These locally appearing phenomena may persist over a significant time and possess a spatial long range memory, which might, thereby, modify the dynamics of an *ensemble of granules* or the granulation dynamics *as a whole*.

In order to investigate granulation dynamics as a whole, we consider the granules intersected by the spectrograph slit as the components of a *complex system*, which can be modulated by oscillations. The granules are organized in a network and respond

to disturbances (for example oscillations) in a linear as well as in a non-linear way (cf. Wachter 2004). It is this networking that determines the system as whole (cf. Richter & Rost 2002).

As we are interested in the behavior of this complex system, we do not try to separate convective and oscillatory motions. We assume, furthermore, that the granulation considered as a stochastic process (turbulent convection) does not change its global behavior with position in the non-active regions, at least in the center of the solar disc.

To probe how locally appearing dynamical events of convective origin affect the dynamics of the complex system we follow the temporal evolution of suitable *global parameters*: $I_{\rm rms}$, $v_{\rm rms}$, $w_{\rm rms}$ (the rms of the observables I, v, w along the slit), and the velocity-intensity correlation $C_{\rm cor}^{\langle {\rm Iv}\rangle}$.

Dynamical events like the fragmentation of large granules in the overshoot layers reported by Mehltretter (1978) might be analogous to the relaxation from a critical state, way out of balance, of a large complex system with many components. In such a critical state minor disturbances may lead to events called avalanches of all sizes (Bak 1996). A system in a self-organized critical state is characterized by a scale-free distribution over the sizes s of avalanches. This implies a power law distribution in the form of $P(s) \propto s^{-\tau}$ (cf. Bak 1996; Jensen 1998).

In the granular system, avalanches (i.e., fragmentation) might be initiated by oversized granules. To investigate this possibility, we make use of the concept and methods of self-organized criticality first proposed by Bak et al. (1987, 1988) and look for scale-free regions in the power spectra of the granular velocities.

In this context the question arises whether the physical states in the deeper and higher layers are represented by the same power law in the scale-free regions. Different power laws would infer different structuring of the layers.

Kinetic energy and flux related to the granular structures as functions of height might indicate the end of convective energy transfer. We approach this question by means of a semi-empirical model of the granular velocity variation with height and combine it with rms velocity measurements at different photospheric heights. Hence, we quantify observationally the different roles that the lower and higher photospheric layers play for the energetics of the convective overshoot.

In a first step we follow the evolution of the basic system observables mentioned above. They are scalar quantities, namely the rms values of the gas velocity v (as measured from Doppler shifts at line center), line width w and continuum intensity I.

In a second step we calculate the power spectrum of the gas velocity v determined at different photospheric heights by means of absorption lines of different strengths.

In a third step we consider globally the variation of the energy of the complex system (as defined above) and its flux with time and height in the photospheric overshoot layers.

2. Material

The current investigation is based on a series of high spatial resolution spectrograms taken on 30 July 1999 with the German Vacuum Tower Telescope (VTT) at the Observatorio del Teide (Tenerife). The spectrograms exhibit an intensity contrast of 5–8%, indicating seeing conditions varying between good and excellent.

The spectrogram series was taken at a fixed position near the center of the solar disk with a sampling rate of 15 s, covering about 20 min in total. The wavelength range was $\lambda\lambda$:491.00–491.40 nm and included several absorption lines of different strength. The slit length corresponds to 130 arcsec, the width to 0.27 arcsec. The slit was oriented in an east-west direction. For more details and an example spectrogram see Nesis et al. (2002). The time series is interrupted twice for 160 s at the 240th and 600th second during the observation.

Table 1. Standard deviation (rms) of the gas velocity observations (Spectrogram 66) at different heights in the photosphere (cf. Sect. 2) as well as the spectroscopic properties of the lines used (Moore 1933).

	$\lambda\lambda^a$	$g_{\rm eff}^b$	H^c	$v_{\rm rms}{}^d$	$I_{\rm rest}{}^e$
unid.	491.31	–	80	740	83
Fe I	491.25	1.04	100	654	86
Fe Ip	491.15	1.25	130	609	72
Fe I	491.18	1.50	180	566	51
Ni I	491.20	0.00	200	578	49
Ti II	491.12	1.10	230	600	50

[a] Wavelength in nm; [b] Landé factor; [c] line formation height in km; [d] gas velocity in m/s; [e] residual intensity in %.

The spectrograms were recorded by a Xedar CCD camera with 2048×2048 pixel, operated in frame selection mode, with an exposure time of 600 ms. By binning 2×2 pixel and further averaging over two adjacent image rows along the slit we obtained a spatial sampling of 0.26 arcsec per pixel and a spectral resolution of 0.23 pm per pixel.

We decided to observe without a correlation tracker, because of the lack of a usable lock point, for example a pore, in the very quiet region that we observed. In this case the correlation tracker may jump to different granules while updating the lock point.

From these spectrograms we obtained the fluctuations of three characteristic observables; namely, the line of sight velocity v, measured as Doppler shift of the line core with respect to the mean profile, the line width FWHM (full width at half minimum), and the continuum intensity I, at equidistant positions s along the spectrograph slit.

The line formation heights were obtained from the contribution function maxima of the line center depression (see Magain 1986, Eq. (21)). The contribution functions were calculated for the photospheric model of Holweger & Müller (1974), assuming LTE.

To check the temperature sensitivity of the absorption lines used, we calculated the line profiles with different models of the temperature in the solar photosphere. We verified that the lines have a small temperature sensitivity, as expected for neutral metal lines of ca. 4 eV excitation energy.

Because we observed a quiet region and the absorption lines have small to moderate Landé factors, they should not be influenced much by magnetic fields. Since moreover the line asymmetry is negligible, any line broadening reflects an unresolved photospheric velocity field w, which may well include photospheric turbulent velocity fluctuations. Thus in the following we will refer to w as line width (or broadening) in velocity units as opposed to the granular convective velocity v. In this paper we make no attempt to filter out wave motion because we investigate here the granulation along the slit as a complex system that may depend on scales significantly larger than the diameters of typical individual granules. (cf. Sect. 1).

In Table 1 we see the spectroscopic properties wavelength (from Moore et al. 1966) and the corresponding Landé factor $g_{\rm eff}$ (calculated using Moore 1933; and Stix 2002a, Eq. (3.54)).

3. Methods

3.1. Global approach

Dynamical variation of the complex granulation system with time. To study the dynamics of the granulation as a whole we needed some global parameters that can be expected to represent the dynamical behavior of the granular sample. We used the rms values of the observed line of sight velocity $\left\langle v^2 \right\rangle^{\frac{1}{2}}$, line width $\left\langle w^2 \right\rangle^{\frac{1}{2}}$, continuum intensity $\left\langle I^2 \right\rangle^{\frac{1}{2}}$, and the intensity-velocity correlation $\langle I\, v \rangle$, which we denote by $v_{\rm rms}$, $w_{\rm rms}$, $I_{\rm rms}$, and $C_{\rm cor}^{\langle {\rm Iv} \rangle}$, respectively. We determined these parameters as functions of time over the entire observation. This enables us to trace the global behavior of the time evolution of the complex system that the granulation represents (cf. Sects. 1 and 2).

The cross-correlation $C_{\rm cor}^{\langle {\rm Iv} \rangle}$ as a global parameter is suited to study the efficiency of the granular convection: $C_{\rm cor}^{\langle {\rm Iv} \rangle}$ is indirectly a function of the temperature fluctuations on the solar surface, and thus of the convective energy flux, which consists mainly of the enthalpy flux (e.g., Böhm-Vitense 1989). Wave motions may also contribute to the energy flux.

The global parameter intensity contrast $I_{\rm rms}$ depends on the one hand on the granular activity, but on the other hand it reacts sensitively to changes of the intensity gradients at the granular borders and thus also to length changes of the intensity structures.

To avoid any influence of possible small-scale magnetic fields, we normally (unless noted otherwise) obtain the observables (v, w, I) from the medium strong absorption line Ni I λ491.20 nm, which has a Landé factor $g_{\rm eff} = 0$. (cf. Table 1). The other lines are only used in the analysis of power spectra and the height dependence of energy terms.

Topological variation of granular structures with time. To describe the evolution of the granular topology over time, we investigated the integral scale F from the statistical description of turbulence (cf. Tennekes & Lumley 1992). The value of F is a rough measure of the interval over which a fluctuating function is correlated with itself. In the following we describe the calculation of the global parameter F for the velocity fluctuations $v(s)$ at various positions s along the spectrograph slit.

By autocorrelation we denote the correlation between the values v at different positions along the slit, $\langle v(s)v(s')\rangle$. Bearing in mind that v is invariant with respect to s, the autocorrelation $\langle v(s)v(s')\rangle$ depends only on the distance between the two positions s and s', i.e., on the spatial *lag* $\tau = |s' - s|$.

For space invariant variables, $\langle v(s)v(s+\tau)\rangle = \langle v(s)v(s-\tau)\rangle$, and it is convenient to define the *autocorrelation coefficient* $r(\tau)$ by

$$r(\tau) = r(-\tau) \equiv \frac{\langle v(s)v(s+|\tau|)\rangle}{\langle v^2(\tau=0)\rangle} \quad \text{with } |r| \leq 1 = r(0). \tag{1}$$

The *integral scale* F is defined by

$$F \equiv \int_0^{\min(r)} r(\tau)\, {\rm d}\tau. \tag{2}$$

As illustrated in Fig. 1, F corresponds to the integration of the autocorrelation up to its first minimum, when the velocity pattern begins to repeat, and measures the area under the $r(\tau)$ function. Because the autocorrelation $r(0) = 1$, F is also roughly the length over which v is correlated with itself, i.e. the equivalent width of the autocorrelation.

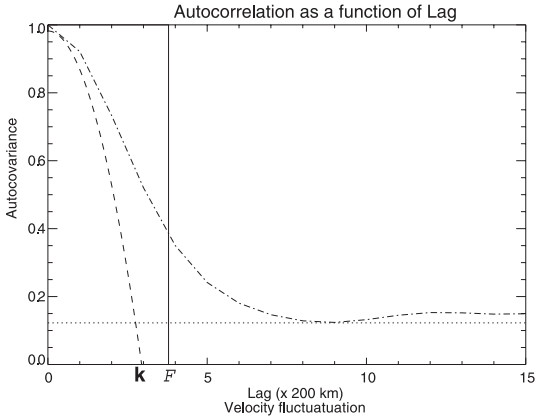

Fig. 1. Autocorrelation $r(\tau)$ of a granular observable (dash-dotted line) and the associated derived measures: integral scale F (which is marked by the solid line) and the Taylor microscale $\boldsymbol{k}$, which is defined by the intersection of the curvature parabola (dashed line) of the autocorrelation coefficient at lag $\tau = 0$ with the abscissa (cf. Tennekes & Lumley 1992). The lag τ is given in units of 200 km, a typical resolution element.

So, F is the global parameter approximating the length of a mean structure along the slit; its variation with the observing time reflects the change of the structure sample and indirectly the change of the granular activity. A noteworthy fact is that the 5-min oscillation velocity field – in the case of large spatial wavelength relative to the granulation – modulates only the amplitude of the convective velocity field (cf. Mattig et al. 1969).

To study the evolution of the intensity and velocity of granular structures we determined the parameters $F_{\rm I}$ and $F_{\rm v}$ with time, respectively.

To qualify the influence of seeing we use a comparative method. Seeing blurs the sharp borders of granular intensity structures. The two global variables $F_{\rm I}$ and $I_{\rm rms}$ are both sensitive to such a variation of the borders. Thus, they are compared over time by inspection. (The gaps in the time series during the intervals [240, 400] and [600, 760] prevent us from using the correlation between $F_{\rm I}$ and $I_{\rm rms}$ as a quantitative measure.)

3.2. Variation of the velocity power with height at different times

To investigate the vertical transfer of the kinetic energy associated with the complex system as a function of spatial scales Λ we consider the velocity power $P_v(k)$ as a function of the wavenumber $k = 2\pi/\Lambda$.

The integral of the function $P_v(k)$ over k yields the mean kinetic energy per unit mass along the slit. The shape of the function $P_v(k)$ determines the amount of energy carried by each spatial scale $\Lambda = 2\pi/k$, respectively.

To trace the variation of the kinetic energy of the system with height in the photosphere we determine the velocity v and the associated kinetic energy distribution by means of six absorption lines representing different heights within the first 200 km above the continuum $\tau_{500} = 1$ (cf. Table 1).

The shape of the function $P_v(k)$ is also indicative of the dynamical processes controlling the small scales. By using lines of various strength we are able to probe the change of the dynamical state within the deep photospheric layers.

All these data are calculated for various times during the observation.

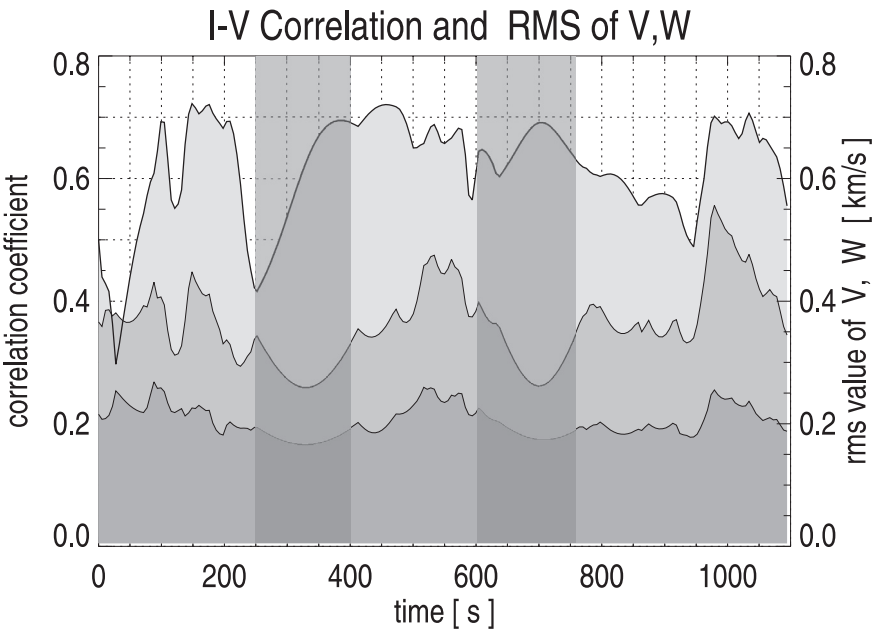

Fig. 2. Time variation of the cross correlation between intensity I and velocity v along the spectrograph slit (upper curve, light gray). Temporal variation of the standard deviation of the line of sight convective velocity v (middle curve, medium gray) and of the line width w (lower curve, dark gray). *Abscissa:* time in seconds; *ordinate left:* cross-correlation value; *ordinate right*: velocity in km s^{-1}. Because of moments of inferior seeing conditions we missed a few measurements in each of the time intervals [250, 400] and [600, 760] (shaded gray), which we replaced by interpolated values. (The interpolation was only used for the graphical presentation of the data in Figs. 2–5 and does not enter the quantitative analysis and physical interpretation.)

3.3. Energy flux density associated with the complex system as a function of height in the deep photosphere at different times

The energy flux density that is convectively transported by the granulation consists of several terms. By far the largest of them is the enthalpy flux, which is therefore often simply called "convective flux". A smaller, but still significant contribution is provided by the kinetic energy flux. Both of these fluxes are carried by eddies covering a large range of scales and velocities, both upward and downward. In addition, superimposed wave motions may also contribute to the energy transport. A full determination of these fluxes would require knowledge of the fluctuations of temperature, velocity, and density over all possible scales, and of correlations between these quantities. Such knowledge is not available. But we will show in this paper that from our observations, when combined with literature data, one can derive useful *upper limits* of these energy fluxes and their variation with height in the solar photosphere.

Velocity as a function of height. To determine the height dependence of the granular line of sight velocity, we have plotted our measured rms velocities $v_{\rm rms}$ as functions of the formation height z of the respective lines (cf. Table 1), for times of different seeing conditions. As is discussed in Sect. 4.3, the results agree nicely with the parametric model velocity variation $v_{\rm mod}(z, A)$ given by Nesis (1985) and Nesis & Mattig (1989). Since the latter has the advantage to extend down to the $\tau_{500} = 1$ level, we use this model velocity $v_{\rm mod}$ for our estimates of the energy densities and fluxes. The parameter A will be defined in Sect. 4.3.

Kinetic energy and its flux density. For these velocities, we calculated the kinetic energy density, $\frac{1}{2}\rho(z)v^2_{\rm mod}(z, A)$, where typical values of the mass density ρ were taken from the model photosphere C of Vernazza et al. (1981), approximated by $\rho(z) = 2.83 \times 10^{-4} \exp(-z/160\,{\rm km})\,{\rm kg\,m^{-3}}$. (Differences between granular and intergranular densities are neglected for our simple estimation.) The kinetic energy is carried upward or downward with the respective velocity, and the net effect of these contributions represents the total kinetic energy flux. Obviously, a conservative upper limit for this flux can be estimated by assuming unidirectional transport at the observed average velocity, so this upper limit is given by $\frac{1}{2}\rho(z)v^2_{\rm mod}(z, A)v_{\rm mod}(z, A)$.

Temperature fluctuations with height in the photosphere. To trace the temperature fluctuations $\langle\delta T\rangle$ with height in the photosphere, we adopted a model of photospheric temperature fluctuations $\langle\delta T\rangle$ given by Kneer et al. (1980, Fig. 4). In this model, the lower ([0, 50] km) and upper ([70, 300] km) parts of the photosphere are treated separately.

Enthalpy flux density. Given this variation of the temperature fluctuations, we can calculate an upper limit for the enthalpy flux density as $\rho\, v_{\rm mod} c_{\rm p} \overline{\Delta T}$ (e.g., Böhm-Vitense 1989, Eq. (14.51)). We used the model temperature fluctuations $\langle\delta T\rangle$ after Kneer et al. (1980), the specific heat at constant pressure $c_{\rm p}$ calculated by Stix (2002, Fig. 2.4), the model velocity $v_{\rm mod}$ given by Nesis (1985) and Nesis & Mattig (1989), and the density from model photosphere C of Vernazza et al. (1981).

4. Results and discussion

4.1. Global evolution of the granular dynamics

Standard deviations (rms) of granular velocity, line broadening and velocity-intensity correlation. Figure 2 shows the evolution of the global parameter $C_{\rm cor}^{\langle {\rm Iv}\rangle}$, the correlation between the line core velocity v of the Ni I line and the continuum intensity I over the observing time. The other two plots show the temporal behavior of the global parameters $v_{\rm rms}$ and $w_{\rm rms}$, the standard deviations (rms) of velocity and line broadening, respectively.

The parameter $C_{\rm cor}^{\langle {\rm Iv}\rangle}$ reflects the degree of structure similarity between v and I along the slit. The correlation values of about 0.7 in the time intervals [100, 240], [400, 600] and [980, 1080] demonstrate the persistently good seeing conditions during these time intervals.

The temporal variations of the standard deviations $v_{\rm rms}$ and $w_{\rm rms}$ reflect the fluctuations of the v and w amplitudes along the slit, respectively. Figure 2 shows that the global

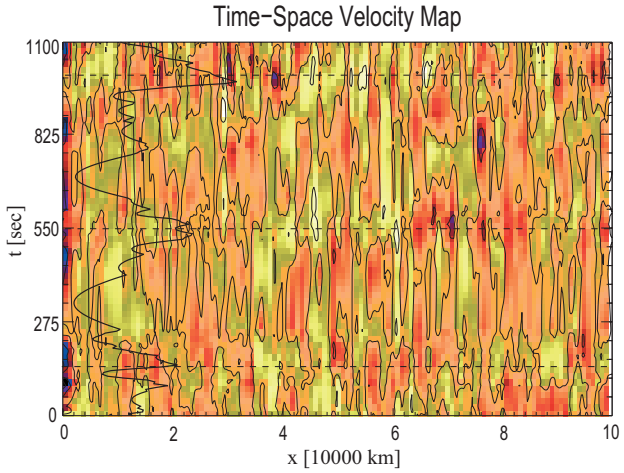

Fig. 3. Time-space map of the gas velocity v (measured as Doppler shift of the core of the nonmagnetic line Ni 491.2 nm, formed at a height of 200 km), overlaid by its standard deviation $v_{\rm rms}$ as a function of time (in arbitrary units; cf. Fig. 2 for numbers). The abscissa is the position along the slit, while the time runs vertically. Yellow color: strong upward velocity (maximum +1.9 km s^{-1}). Dark blue color: strong downward velocity (minimum –1.44 km s^{-1}). Dashed lines mark instants of large $v_{\rm rms}$.

parameters $v_{\rm rms}$ and $w_{\rm rms}$ vary synchronously with time in the above mentioned intervals. There, they show burst-like variations, while the parameter $C_{\rm cor}^{\langle {\rm Iv}\rangle}$ remains constant.

It is remarkable that the value of $C_{\rm cor}^{\langle {\rm Iv}\rangle}$ rarely exceeds the 0.7 level, even at an excellent observing moment such as around the 980th second, when the intensity contrast rose to 8% (cf. Fig. 5). The correlation value depends on the matching of the velocity and intensity spatial structures. Evidently the matching is not perfect, e.g. the emergence of maximum granular velocity does not necessarily correspond to an intensity maximum (cf. Nesis et al. 2002). Therefore a reduced correlation is observed.

The values of $v_{\rm rms}$ vary over the time from $\leq$0.3 to $\geq$0.5 km s^{-1}. The time difference between the maxima is approximately 450 s (7.5 min).

The strong temporal coincidence of $w_{\rm rms}$ and $v_{\rm rms}$ (cf. Fig. 2), especially at times when $v_{\rm rms}$ rises to higher values, is particularly interesting. The similar behavior of $w_{\rm rms}$ and $v_{\rm rms}$ in the intervals [100, 240], [400, 600] and [920, 1080] implies a tight dependence of $v_{\rm rms}$ on $w_{\rm rms}$. This dependence is reminiscent of the enhancement of the line broadening $w_{\rm rms}$ at the granular borders as a response to the steep granular velocity gradients there (cf. Nesis et al. 1999).

To see the time variation of the global parameter $v_{\rm rms}$ in the context of the history of the local gas velocity fluctuations along the spectrograph slit, we plot $v_{\rm rms}$ on the time-space map of the corresponding v fluctuations (cf. Fig. 3). Here the large values of $v_{\rm rms}$ reflect strong fluctuations (yellow or dark blue color) of the gas velocity measured from line center Doppler shifts along the slit. To demonstrate this, we draw lines parallel to the horizontal axis (i.e., the slit) through prominent maxima of $v_{\rm rms}$.

Concerning physical processes underlying and modifying the granulation dynamics, the velocity bursts in Fig. 2 could be seen either as a result of a modulation of the convective velocities by wave motion or as events due to the stochastically repeated emergence of convective bursts or downward plumes at various places along the slit during the observation.

It is remarkable that the interval between the maximum values of the repeated bursts of $v_{\rm rms}$ in Fig. 2 is ≈450 s. According to Komm et al. (1991b, Fig. 6b) the deep photospheric layers have a Brunt-Väisalä frequency of about 420 s. Puschmann et al. (2003) interpret the measured phase shifts between gas velocity and continuum intensity as possible evidence of gravity waves in the photospheric layers. Other processes that are able to globally modify the granulation dynamics could be the collapse of individual granules in layers deeper than $\tau_{500} = 1$ (cf. Skartlien 1998) or downward plumes (cf. Rast 2003). There is insufficient evidence to choose one of the three explanations for the temporal behavior of $v_{\rm rms}$.

Velocity and intensity spatial scales of granulation. Figure 4 shows the evolution of the global parameter $C_{\rm cor}^{\langle {\rm Iv}\rangle}$ and the integral scales $F_{\rm I}$ and $F_{\rm v}$ over the observing time (cf. Sect. 3.1). $F_{\rm v}$ (medium gray) fluctuates between 700 and 1350 km with an average of ≈900 km. $F_{\rm I}$ (dark gray) shows moderate changes between 520 and 900 km around an average of ≈700 km. $C_{\rm cor}^{\langle {\rm Iv}\rangle}$ remains nearly constant at the 0.7 level.

$F_{\rm v}$ and $F_{\rm I}$ fluctuate around different mean scales ≈900 km and ≈700 km, respectively. This implies that the granular velocity scale is ≈1.3 times larger than the intensity scale over the observation.

The temporal behavior of $F_{\rm v}$ changes relative to that of $F_{\rm I}$ in the last 480 s of the observation. As we can see in Fig. 4, $F_{\rm v}$ shows large amplitudes compared to $F_{\rm I}$ within the first 720 s while the amplitudes are similar in the last 480 s. This implies that in the first 720 s of the observation the granular velocity structures tend to be larger than the intensity structures.

The light vertical bars in Fig. 4 indicate particular moments in the evolution of the global parameters $C_{\rm cor}^{\langle {\rm Iv}\rangle}$, $F_{\rm v}$ and $F_{\rm I}$. At the 860 th second the parameter $C_{\rm cor}^{\langle {\rm Iv}\rangle}$ shows a relatively small value (<0.6). This happens despite the similarity between the mean granular intensity and velocity structure expressed by the equality of the integral length parameters $F_{\rm I}$ and $F_{\rm v}$. Since the latter are of similar size, the small value of $C_{\rm cor}^{\langle {\rm Iv}\rangle}$ implies that the maximum of the granular velocities along the slit does not necessarily coincide with the intensity maxima (Nesis et al. 2002).

About 2.5 min later, at the 970th and 1040th seconds, the parameters $C_{\rm cor}^{\langle {\rm Iv}\rangle}$, $F_{\rm v}$ and $F_{\rm I}$ show the opposite behavior. $C_{\rm cor}^{\langle {\rm Iv}\rangle}$ approaches its maximum value ≈0.7, despite the lack of similarity between the mean granular velocity and intensity structures: the integral parameters $F_{\rm v}$ and $F_{\rm I}$ are not equal. This behavior indicates a good correspondence between the velocity and intensity maxima along the slit, which compensate for the lack of similarity in less prominent structures, thereby enhancing the value of the correlation.

The temporal averages of ≈900 km and ≈700 km of the parameters $F_{\rm v}$ and $F_{\rm I}$ are the first moments of the corresponding spatial-temporal distributions. As integral measures they reflect the mean properties of the distribution of the spatial scales of the intensity and velocity along the slit, while their time averages reveal the mean properties of their distribution over the observation.

The fact that the scales for the velocity and intensity structures are different partly explains why the cross-correlation achieves only a maximum level of 0.7.

Intensity contrast and intensity length scale of granulation. In Fig. 5 the time variation of the intensity contrast $I_{\rm rms}$ and the intensity length measure $F_{\rm I}$ are shown. Because both $I_{\rm rms}$

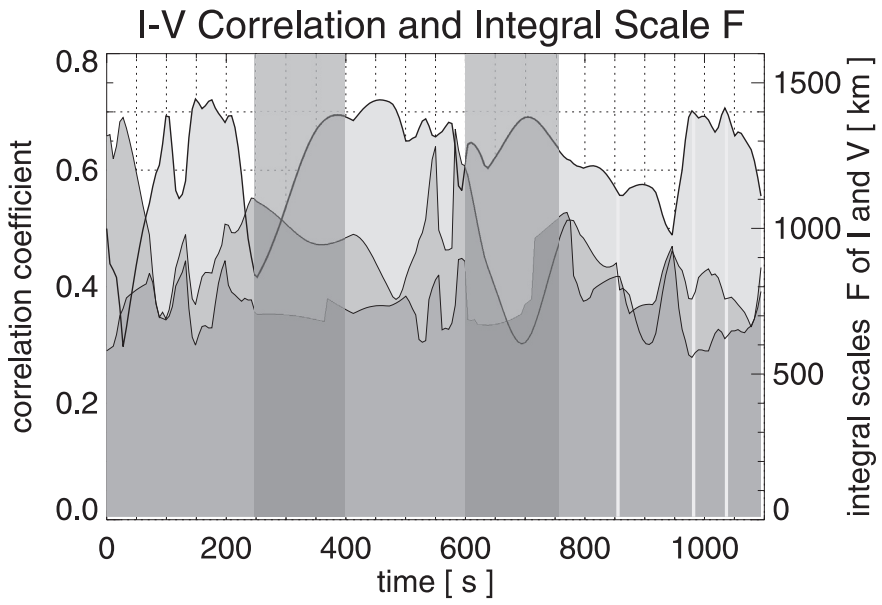

Fig. 4. Time variation of the scale length F for intensity I (lower curve, dark gray) and velocity v (middle curve, medium gray) as well as their cross correlation $C_{\rm cor}^{\langle {\rm Iv} \rangle}$ (upper curve, light gray). *Abscissa:* time in seconds; *ordinate left:* value of cross-correlation; *ordinate right:* length scale F.

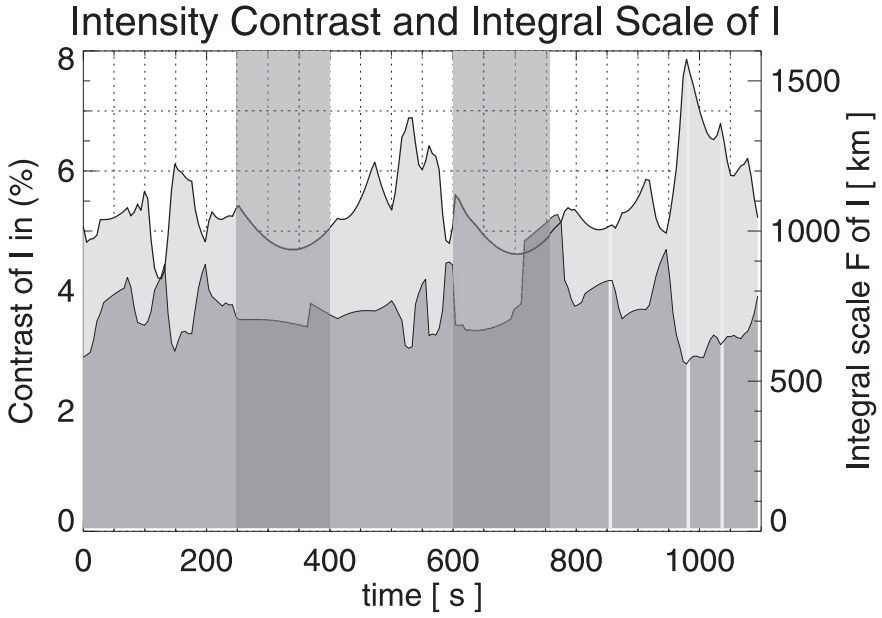

Fig. 5. Time variation of the intensity scale length $F_{\rm I}$ (lower curve, dark gray) as well as the intensity contrast (upper curve, light gray). *Abscissa:* time in seconds; *ordinate left:* intensity contrast value in %, *ordinate right:* length scale $F_{\rm I}$. The vertical bars indicate characteristic moments during the observation.

and $F_{\rm I}$ respond sensitively to variations of seeing conditions we compare their temporal behavior during the observation.

Normally, excellent observational conditions manifest themselves by high contrast (large values of $I_{\rm rms}$) associated with short length scales (small values of $F_{\rm I}$) and vice versa. Thus, under good seeing conditions we expect an opposite behavior of $I_{\rm rms}$ and $F_{\rm I}$ (cf. Sect. 3.1). The light gray vertical bars in Fig. 5 indicate such moments: at the 860 th second the reduced contrast $I_{\rm rms}$ is associated with an enlarged length scale $F_{\rm I}$ while at the 970, 1040 th seconds an enlarged $I_{\rm rms}$ corresponds to a reduced intensity length scale $F_{\rm I}$.

However, the expectation of an anticorrelation between $I_{\rm rms}$ and $F_{\rm I}$ is seen to be not strictly fulfilled. In the time intervals of high $I_{\rm rms}$, which represent optimal seeing conditions, $F_{\rm I}$ varies less rapidly than the contrast and poorly follows its long-term fluctuations. The short-term fluctuations within these time intervals might be due to seeing, but are more likely due to solar effects, which are more visible under better seeing.

Since during the entire observation the seeing quality varied between good and excellent, and because of the overall behavior of the various observed quantities, we think that seeing cannot be the only reason for the variations of $I_{\rm rms}$ in Fig. 5 and for the variation of $v_{\rm rms}$ and $w_{\rm rms}$ shown in Fig. 2.

The intensity contrast $I_{\rm rms}$ (light gray) in Fig. 5 as a function of time follows the burst-like variation of the global parameters $v_{\rm rms}$ (medium gray) and $w_{\rm rms}$ (dark gray) in Fig. 2, while its amplitude varies between ≈4% and 8%. The characteristic maxima of approximately 7% and 8% are separated in time by 450 s.

4.2. Variation of the velocity power with height at different times

In Fig. 6 we see six velocity power spectra $P_{\rm v}(k)$, determined at the same observing time at six different photospheric heights (cf. Table 1). The intensity contrast at this time was 8%.

Figure 6 shows the fanning out of the power functions with height, which is associated with the change of the scaling law $P_{\rm v}(k) \sim k^{-q}$ from $q = -5$ to $q = -7$ for the deepest and highest layers, respectively. The spreading out of the power functions

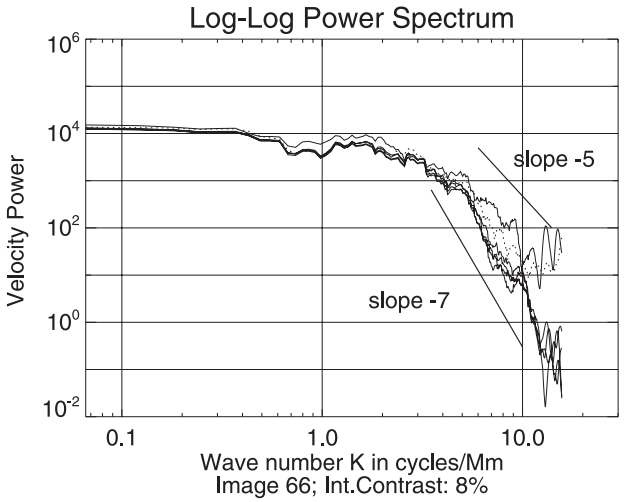

Fig. 6. Power of the velocity fluctuations v along the spectrograph slit as a function of the wavenumber k in log-log presentation. The six functions $P(k)$ reflect the power of velocity fluctuations determined at six different heights in the photosphere. At large wave numbers, their slopes range between –5 and –7 for the deepest and highest layers, respectively, as indicated by the two straight lines. The data are for image No. 66, taken towards the end of the observation (at 990 s).

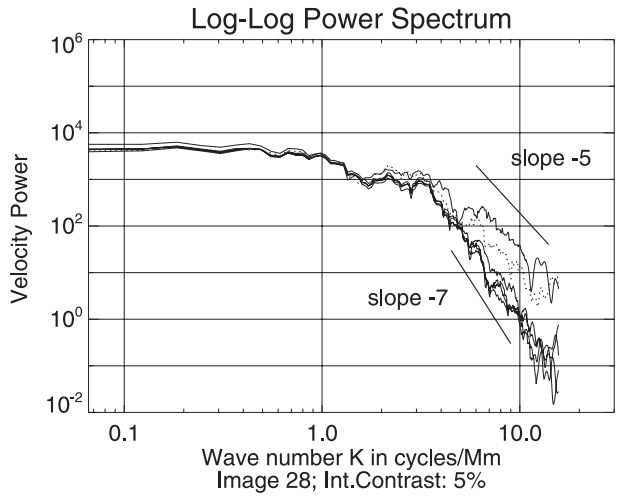

Fig. 7. Power of the velocity fluctuations as in Fig. 6, but for image No. 28, taken at 420 s in the middle of the observation.

involves only the higher wave numbers k beginning at $k \approx 5\,\mathrm{Mm}^{-1}$ ($\Lambda = 2\pi/k \approx 1250\,\mathrm{km}$). So, for wave numbers $\geq 10\,\mathrm{Mm}^{-1}$ the power difference between the deeper and higher photospheric layers is one order of magnitude or more.

Figure 7 exhibits in the same way as Fig. 6 six velocity power spectra, for data recorded about 10 min earlier. At this observing time the intensity contrast was 5%. Nevertheless, the power functions $P_\mathrm{v}(k)$ in Fig. 7 behave in a similar way as the power functions presented in Fig. 6. Again we find a clear separation of the power spectra functions according to their slope at higher wave numbers.

The change of the steepness in the power spectra appears to be observational evidence for the attenuation of the dynamics of the small scales with height in the photosphere: the small fragments produced in the deepest layers lose their dynamics in the higher ones. According to Figs. 6 and 7 this process begins at scales of the order of $\Lambda = 2\pi/k \approx 1250\,\mathrm{km}$ (cf. Krieg et al. 2000; Sánchez Cuberes et al. 2000).

In the framework of the self-organized criticality theory (cf. Bak 1996) we regard the granulation as a large complex system of various spatial scales, with part of them in a critical state - e.g., minor disturbances may drive these scales to avalanches, i.e. to fragmentation. The latter is characterized by a scale-free power distribution $P_\mathrm{v}(k) \propto k^q$.

In the velocity power spectra in Figs. 6 and 7 we find a scale-free power distribution over k in the wavenumber interval [0.4, 1.2] Mm. In this range, the function $P_\mathrm{v}(k)$ takes the form of a power law $P_\mathrm{v}(k) \propto k^q$ with $q = 5{-}7$, depending on the depth in the photosphere.

The limits of the range where the scaling law $P_\mathrm{v}(k) \propto k^q$ applies are determined by the mean granular size (1.2 Mm) and the spatial resolution of our spectra (0.4 Mm). This shows that only small-scale granules (beginning with the order of the mean granular size) can be considered to be in a critical state. Here, the small scales relax by fragmentation or conglomeration and new fragmentation in response to minor disturbances. Thus, the change of the scaling law with the height in the photosphere reflects the change of the fragmentation process with height.

4.3. Velocity, energy and energy flux density as functions of height in the photosphere at different times

Velocity distribution with height above the continuum. In Fig. 8 (left panel) we show the distribution of our rms velocity measurements v_rms with height in the photosphere. The three sets of the six velocity measurements (plotted with various symbols) refer to three different observation moments with 8 to 5% intensity contrast. These measurements can be compared with previous results (cf. Nesis & Mattig 1989, Table 3, lower panel, $\cos\theta = 1$), where velocity measurements were shown to follow a functional relationship given by the parametric model velocity function $v_\mathrm{mod}(z, A) = v_{01}\mathrm{e}^{-z/h_1} + v_{02}\mathrm{e}^{z/h_2}$ (cf. Nesis 1985). The solid and dashed line in Fig. 8 show the runs of the function $v_\mathrm{mod}(z, A)$ with height z for two different parameter sets $A = [v_{01}, h_1, v_{02}, h_2]$. For the solid line we used the parameter set $[v_{01} = 1.05\,\mathrm{km\,s^{-1}}, h_1 = 95\,\mathrm{km}, v_{02} = 0.115\,\mathrm{km\,s^{-1}}, h_2 = 270\,\mathrm{km}]$, which is practically equal to values used by Nesis & Mattig (1989). The dashed line is plotted with slightly modified parameters: $[v_{01} = 0.86\,\mathrm{km\,s^{-1}}, h_1 = 85\,\mathrm{km}, v_{02} = 0.10\,\mathrm{km\,s^{-1}}, h_2 = 205\,\mathrm{km}]$.

The plots in Fig. 8 (left panel) show clearly that the variation of the velocity $v_\mathrm{mod}(z, A)$ with height in the photosphere retains its form despite the change of the intensity contrast (8 to 5%); actually, a change of contrast affects the velocity amplitude. Moreover, our new velocity measurements confirm the model $v_\mathrm{mod}(z, A) = v_{01}\mathrm{e}^{-z/h_1} + v_{02}\mathrm{e}^{z/h_2}$ of Nesis & Mattig (1989).

Thus, based on our rms velocity measurements v_rms, the model velocity variation of Nesis & Mattig (1989), and the model temperature fluctuations $\langle \delta T \rangle$ after Kneer et al. (1980), we were able to derive the height dependence of the kinetic energy density and of conservative upper limits of its flux density as well as the enthalpy flux density.

Kinetic energy density as a function of height. Figure 8 (right panel) shows the variation with height of the kinetic energy density $\frac{1}{2}\rho(z)v^2_\mathrm{mod}(z, A)$ associated with the velocity model function v_mod. The solid and dashed line correspond to the two parameter sets A, [1.05, 95, 0.115, 270] and [0.86, 85, 0.10, 205], respectively (as discussed in the preceding paragraph). The symbols

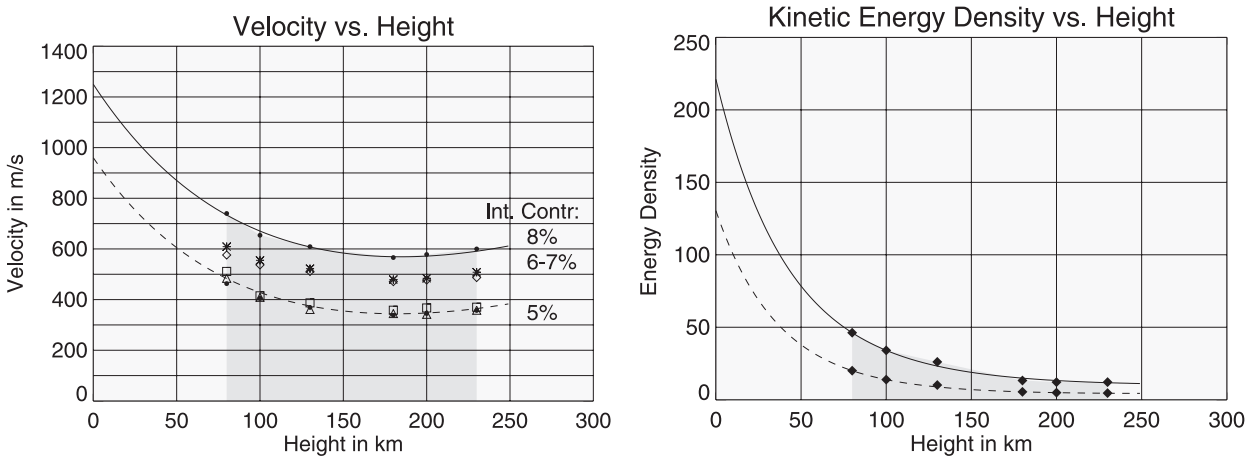

Fig. 8. *Left panel*: parametric model velocity function $v_{\rm mod}(z, A)$ in the photosphere (*solid* and *dashed line*) and sets of measured velocities v (*symbols*) at different heights and at times of different intensity contrast (8 to 5%). The *ordinate* is the velocity in m/s; the *abscissa* represents the height in the photosphere above $\tau_{500} = 1$ in km. *Right panel*: variation of the kinetic energy density with height z in the deep photosphere. The *solid line* and *dashed line* show the model variation $\frac{1}{2}\rho(z)v^2_{\rm mod}(z, A)$ [in $\mathrm{Jm^{-3}}$] for the same parameter sets A as used in the left panel. The symbols represent the kinetic energy density according to our measurements at different heights and observation times corresponding to 8 and 5% intensity contrast, respectively.

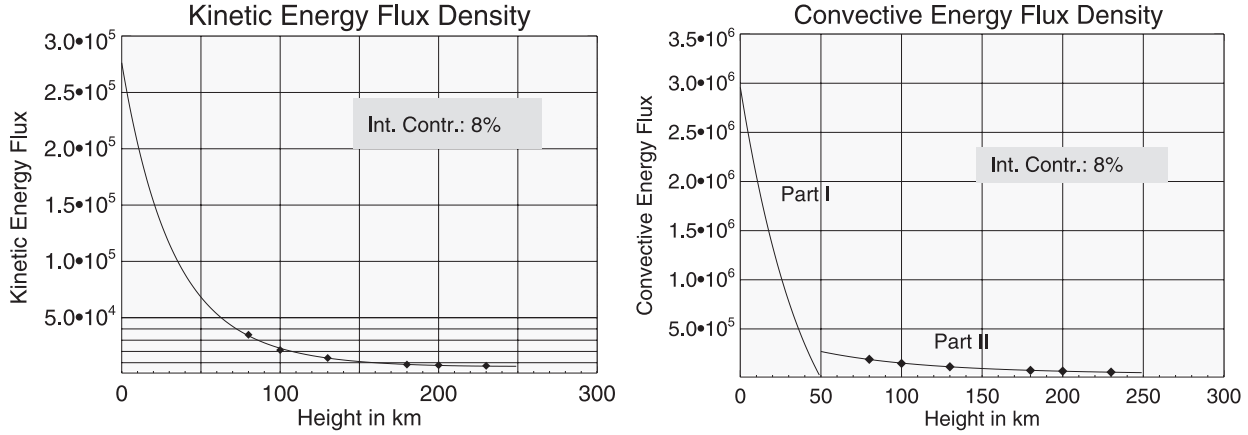

Fig. 9. *Left panel*: variation of the derived upper limit to the kinetic energy flux density [in $\mathrm{J\,m^{-2}\,s^{-1}}$] with height z in the deep photosphere. The symbols represent the energy flux measurements at different heights in the photosphere. *Right panel*: as in Fig. 9 (*left panel*) but for the enthalpy flux density $\rho\, v\, c_{\rm p}\overline{\Delta T}$ [in $\mathrm{J\,m^{-2}\,s^{-1}}$]. The symbols represent the enthalpy flux measurements at different heights in the photosphere, while the drawn curves refer to the parametric model.

represent the kinetic energy at different heights and observation times corresponding to 8 and 5% intensity contrast, respectively.

The variation of the plots in Fig. 8 (right panel) reflects not only the behavior of $v_{\rm mod}$ with height (cf. left panel) but also of the density $\rho(z)$. As a result of the latter dependency, the kinetic energy density function becomes very flat at larger heights, in particular above 150 km. In the layers just above $\tau_{500} = 1$, however, the function $\frac{1}{2}\rho(z)v^2_{\rm mod}(z, A)$ slopes down very steeply: the energy drops by a factor of four from its value at $\tau_{500} = 1$ within the first 100 km. Therefore, the kinetic energy density corresponding to our rms velocity measurements $v_{\rm rms}$ represents only less than one-quarter of the energy at the continuum height for scales of granular size. Thus, the granulation-like motions practically disappear in the overlying layers within one pressure scale height. This agrees with the result of Nesis et al. (1988) that the intensity structures at scales of the order of the granular size lose their similarity to the continuum also within a pressure scale height.

Enthalpy flux density. Figure 9 (right panel) shows the variation of the upper limit to the enthalpy flux $\rho\, v c_{\rm p}\overline{\Delta T}$ with height z in the deep photosphere. The maximum enthalpy flux is seen to be of the order of a few times $10^6\,\mathrm{J\,m^{-2}\,s^{-1}}$ at the granulation layers near $\tau_{500} = 1$ and drops to $10^5\,\mathrm{J\,m^{-2}\,s^{-1}}$ in the first 50 km above. The strong reduction of the enthalpy with height explains the lack of coherence between the intensity variations at $\tau_{500} = 1$ and one pressure scale higher found by Nesis (1985).

To prove the reliability of our enthalpy calculations we compared our model calculated enthalpy flux at the $\tau_{500} = 1$ layers with the luminosity per square meter and per second at the solar surface. The latter amounts to $6.3 \times 10^6\,\mathrm{J\,m^{-2}\,s^{-1}}$ (cf. Allen 1973), which corroborates our estimates.

5. Conclusion

The present investigation addresses three different aspects of granulation: the *temporal evolution* of the dynamics and topology at various scales, the *power law* expressing the velocity power spectrum, and the associated *energy transfer*.

The temporal evolution of granulation dynamics shows a practically synchronous variation of $v_{\rm rms}$, $w_{\rm rms}$, and $I_{\rm rms}$ in the form of repeated bursts with a typical repetition time of 450 s.

As discussed above, this variation seems to be caused not only by seeing effects. Thus the question arises about the nature of the underlying solar processes generating this form of variation.

Possible candidates are either wave motions with a Brunt–Väisalä frequency of about 420 s, or single local events like a collapse of a granule in layers deeper than $\tau_{500} = 1$, or downward plumes at the granular borders; each of them would influence the granulation as a whole.

The time variation of the granular topology shows that the velocity length scale $F_{\rm v}$ is on average 1.3 times larger than the intensity length scale $F_{\rm I}$ over the whole observation; a result that can partially be due to seeing influence on the intensity scales. Remarkable is, however, the finding that the parameters $F_{\rm v}$ and $F_{\rm I}$ show only a partially uniform evolution, despite the fact that both are measures of the convective structures.

The height variation of the velocity power reveals the existence of *a threshold scale* (of about 200 km) in the deep photosphere. At this scale the power changes as a function of scale, both in its slope and in its behavior with height.

We find that the large scale power remains practically constant and does not show any change with height. In contrast, with increasing height in the photosphere the power associated with small scales is reduced drastically towards smaller scales, implying the disappearance of small scales in the higher photospheric layers. This behavior remains the same at different times.

Despite the complexity of the granulation as a whole, it is remarkable that only for small scales is the power distributed according to a *power law,* inferring thus a state of self-organized criticality of the small granules.

The energy flux drops impressively (by a factor of 10) within the first 100 km above $\tau_{500} = 1$ and continues to fall moderately within the layers above. This infers that the bulk of the energy flux disappears within one pressure scale height, while the rest is transfered to the higher layers by structures larger than the threshold scale.

Taken together, our empirical and semi-empirical findings confirm some previous results on the granular dynamics, but present also new aspects of the nature of the small scales in the solar granulation.

Acknowledgements. We are grateful to W. Dobler and L. Bellot Rubio for helpful comments. The work of M.R. was supported by DFG grant STI 6519. The constructive comments of the anonymous referee are highly appreciated.

References

Allen, C. W. 1973, Astrophysical Quantities, University of London (The Athlone Press)
Bak, P. 1996, How Nature Works (New York: Springer-Verlag)
Bak, P., Tang, C., & Wiesenfeld, K. 1987, Phys. Rev. Lett., 59, 381
Bak, P., Tang, C., & Wiesenfeld, K. 1988, Phys. Rev. A, 59, 364
Borrero, J. M., & Bellot Rubio, L. R. 2002, A&A, 385, 1056
Böhm-Vitense, E. 1989, Stellar Astrophysics (Cambridge University Press), 2, 185
Holweger, H., & Müller, E. 1974, Sol. Phys., 39, 19
Jensen, H. J. 1998, Self-Organized Criticality (Cambridge University Press)
Kneer, F. J. R., Mattig, W., Nesis, A., & Werner, W. 1980, Sol. Phys., 68, 31
Komm, R., Mattig, W., & Nesis, A. 1991a, A&A, 243, 251
Komm, R., Mattig, W., & Nesis, A. 1991b, A&A, 252, 827
Krieg, J., Kneer, F., Koschinsky, M., & Ritter, C. 2000, A&A, 360, 157
Magain, P. 1986, A&A, 163, 135
Mattig, W., Mehltretter, J. P., & Nesis, A. 1969, Sol. Phys., 10, 254
Mehltretter, J. P. 1978, A&A, 62, 311
Moore, C. E. 1933, A Multiplet Table of Astrophysical Interest, Princeton, N.J.
Moore, C. E., Minnaert, M. G. J., & Houtgast, J. 1966, The Solar Spectrum 2935 Å to 8770 Å, National Bureau of Standards Monograph, 61
Muller, R. 1999, in ed. A. Hanslmeier, & M. Messerotti, Motions in the Solar Atmosphere, Astrophysics and Space Science Library (Kluwer), 239, 35
Nesis, A. 1985, Dissertation, TU Berlin
Nesis, A., Durrant, C. J., & Mattig, W. 1988, A&A, 201, 153
Nesis, A., & Mattig, W. 1989, A&A, 221, 130
Nesis, A., Hammer, R., Hanslmeier, A., et al. 1997, A&A, 326, 851
Nesis, A., Hammer, R., Kiefer, H., et al. 1999, A&A, 345, 265
Nesis, A., Hammer, R., Roth, M., & Schleicher, H. 2002, A&A, 396, 1003
Nesis, A., Hammer, R., & Schleicher, H. 2003, Astron. Nachr., 324, 55
Puschmann, K., Vázquez, M., Bonet, J. A., Ruiz Cobo, B., & Hanslmeier, A. 2003, A&A, 408, 363
Rast, M. P. 2003, ApJ, 597, 1200
Richter, K., & Rost, J.-M. 2002, Komplexe Systeme, Fischer Taschenbuch Verlag
Sánchez Cuberes, M., Bonet, J. A., Vázquez, M., & Wittman, A. D. 2000, ApJ, 538, 940
Skartlien, R. 1998, Ph.D. Thesis, Univ. Oslo
Stix, M. 2002, The Sun, 2nd edn. (Springer-Verlag), 37
Tennekes, H., & Lumley, J. L. 1992, A first Course in Turbulence, 14th edn. (MIT Press), 210
Vernazza, J. E., Avrett, E. H., & Loeser, R. 1981, ApJS, 45, 635
Wachter, R. 2004, Dissertation, ETH Zürich, No. 15514